PROGRESSIVE FATIGUE DAMAGE IN 3D MODIFIED LAYER-TO-LAYER WOVEN COMPOSITES CHARACTERISED BY X-RAY TOMOGRAPHY

B. Yu[a], J. Stein[b], F. Leonard[b], P. J. Withers[b*], C. Soutis[a]

[a] *Northwest Composite Centre, School of Materials, University of Manchester Manchester M13 9PL*
[b] *Henry Moseley X-ray Imaging Facility, School of Materials, University of Manchester Manchester M13 9PL*
[*] *philip.withers@manchester.ac.uk*

Keywords: damage development, X-ray CT, 3D woven composites, fatigue.

Abstract
This study investigates the development of fatigue damage in 3D woven composites reinforced with a modified layer-to-layer glass fibre preform, exploring the effect of fibre architecture on damage evolution. The results obtained from the mechanical tests were supplemented by the progressive damage observation using X-ray computed tomography (CT). It was found that the fatigue damage initially occurs in the form of transverse cracks. Subsequently at higher numbers of fatigue cycles, the transverse cracks started splitting at the cross-over area, accompanied by interfacial debonding cracks between adjacent binder yarns (delamination). Finally, the detachment of binder yarns gave rise to extensive damage.

1. Introduction

Recently, three-dimensional (3D) woven composites have gained a growing research interest for a wide range of industrial applications, due to their superior interlaminar properties over 2D laminates. The through-thickness reinforcement, provides a bridging effect impeding the spread of delamination cracks. This is counterbalanced by a reduction in in-plane mechanical strength by introducing features such as fibre crimp, geometrical irregularities and polymer rich regions [1-3]. While it is acknowledged that fibre architecture plays a significant role in shaping damage initiation and propagation in 3D woven composites, there is little understanding at present. Consequently there is a need to know how the local micro-structure affects damage formation before they are implemented into service.

To date, many studies have focused on examining damage mechanisms either using optical and electronic microscopy for prepared sections [4, 5], or using indirect techniques such as acoustic emission or infra-red to register damage events [6, 7]. X-ray computed tomography (CT) has demonstrated its advantages in the evaluation of materials non-destructively, particularly in characterising damage evolution, while the sample integrity is well preserved [8]. Lambert et al. [9] studied the influence of voids on fatigue performance, aiming to conduct continued testing to focus on damage accumulation in one sample. However, the

resolution obtained for full cross-section scans failed to resolve micro-scale damage. As a result, different samples were damaged to different extents and were sectioned afterwards [9].

In our previous study, we developed a quantitative method for segmenting the different fatigue damage modes in a 3D modified layer to layer composite material [10]. This study aims at tracking the damage accumulation throughout the fatigue life by repeated non-destructive X-ray computed tomography.

2. Materials and Experimental methods

2.1 Materials fabrication

The 3D woven fabric was produced by a conventional rapier weaving machine equipped with an electronic jacquard shedding. The fibre material was 660 tex S-2 glass yarns. The schematic illustration of the 3D modified layer-to-layer fibre architecture is shown in Fig.1, where the weft yarns appear in blue and binder yarns are shown in red. As illustrated in Fig. 1, there is no in-plane warp yarn in the fabric. Instead binder yarns were woven into the warp direction, bonding two neighbouring layers of weft yarns together. This architecture is modified to reinforce the free surfaces at the top and bottom, with additional binder yarns interlaced into the structure, which are shown in yellow.

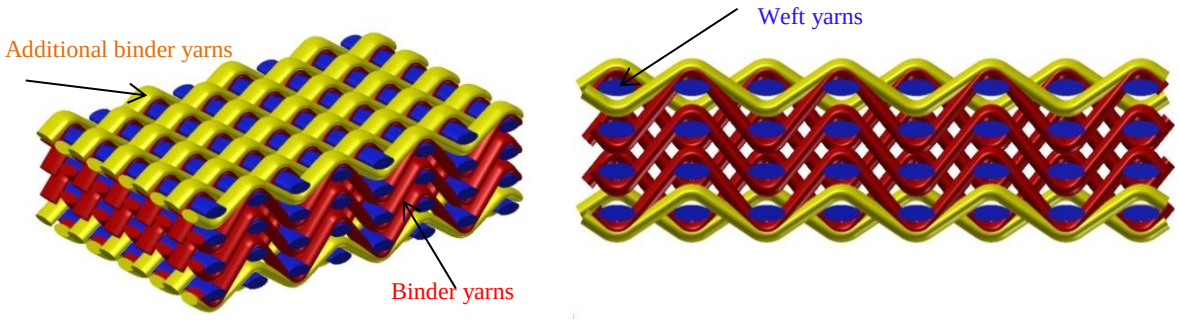

Figure 1. Schematic illustration of the idealised fibre architecture of 3D modified layer-to-layer preform

The composite panels were manufactured by infusing the 3D woven preform with LY564 epoxy resin and XB3486 hardener, using vacuum assisted resin infusion process. The panel was then cured at 80° for 8 hours, under 1 atmosphere of pressure (only vacuum pressure, no applied pressure). The 130mm × 16mm specimens, were cut out from the composite panel using a diamond saw. 50mm long GFRP (glass fibre reinforced polymer) end tabs were bonded on each end of specimen, resulting in a 30mm gauge length. Noting that the specimens are smaller than the standard size recommended in ASTM D3039, the effect of the specimen dimensions on mechanical behaviour must be taken into consideration. Therefore, static and fatigue tensile tests were conducted on the small and standard size specimens. The testing procedures are described as follows.

2.2 Mechanical testing

Static tensile tests were performed on the modified layer-to-layer specimens using INSTRON 5582 machine (load cell 100 kN) with crosshead loading rate of 2mm/min. The strain was measured using an advanced video extensometer. The tensile strength and failure strain were

measured by taking the results from five specimens showing valid failure according to ASTM D3039. An INSTRON 8802 was used for the tension-tension fatigue tests, with an R ratio (minimum to the maximum stress in the cycle) of 0.1 at 5Hz. The applied load level corresponded to 40% of the ultimate tensile strength of 467±35 MPa. In addition, the machine was also used to measure the axial residual stiffness, a useful indicator for registering the extent of damage and for evaluating its influence on mechanical properties [11]. It was measured by interrupting the fatigue test at 0, 10^2, 5×10^3, 10^4, 5×10^4 and 6×10^4 cycles.

2.3 X-ray computed tomography

In order to follow the damage evolution throughout the whole fatigue life, the tension-tension fatigue test was stopped at 10^2, 10^3, 5×10^3, 10^4, 5×10^4 and 6×10^4 cycles, followed by X-ray CT scans on the damaged specimen. To enhance the image contrast, a Zinc-iodide based dye penetrant was employed to fill through the internal cracks in the damaged sample. It was made up of 250g zinc iodide, 80ml distilled water, 80ml isopropyl alcohol and 1ml kodak photoflow. The damaged specimen was soaked in the solution for 24 hours before it was scanned at the Henry Moseley X-ray Imaging Facility using the Nikon Metrology 225/320 kV Custom Bay, using an accelerating voltage of 70 kV and current of 90 µA. 3142 projections were captured as the specimen was rotated over 360°. The exposure time for each was 1s, which resulted in the total acquisition time of 2h37min. The scan volume was $23.6\times23.6\times23.6mm^3$, within which the 16mm wide sample was included. The obtained resolution was 11.8µm. Considering the whole gauge length was 30mm, the field-of-view was not sufficient to cover the whole gauge length. Therefore two scans were performed to capture the full gauge length, allowing enough damage information being collected.

The Nikon Metrology proprietary software CT-pro was used for data reconstruction as well as noise reduction and beam hardening artefact removal. The image processing software VG studio was employed to export reconstructed images and reduce data size. For consistency of contrast the same input grey scale values were used for grey scale redistribution. The float data was converted to the unsigned 8 bit data by remapping the histogram.

3. Results and discussion

It was important to focus on the same region throughout so that damage development could be monitored. The cross-sectional images were taken approximately from the middle of each volume (see Fig. 2), where damage is thought to be insensitive to the sample edges. These cross-sections are shown in Fig. 3 and Fig. 4, which show damage initiation and propagation as well as the interaction of different damage modes as a function of the number of fatigue cycles.

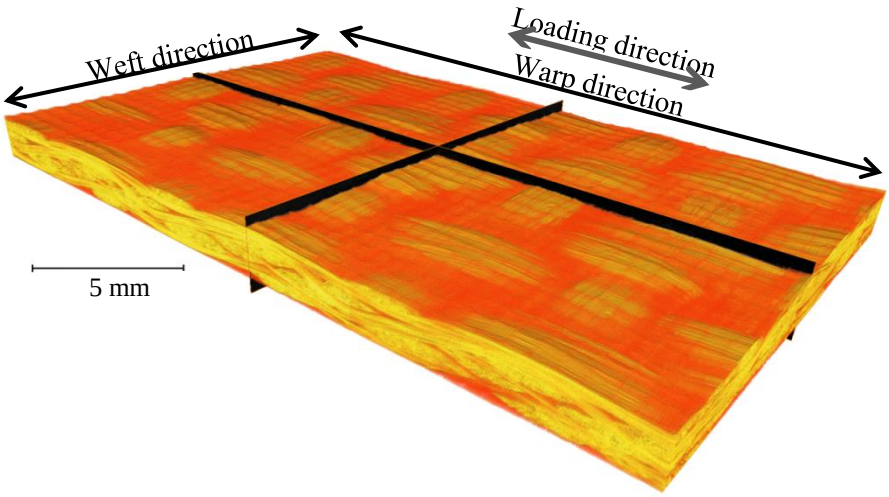

Figure 2. 3D volume rendering of full gauge volume with the 3D glass fabric shown in yellow and the resin semi-transparently displayed in orange.

As shown in Fig. 3(a), no damage is visible prior to fatigue cycling, suggesting that pre-existing microstructural defects can be eliminated as a potential cause of fatigue damage. As shown in Fig. 3(b), transverse cracks within the weft yarns start to initiate in the first 10^2 cycles, with one crack appearing in every four weft yarns. It is of note that only those weft yarns situated close to the surface suffered such damage, which may indicate that the binder yarns at surface are more severely undulating than for the yarns inside. Due to the undulation of binder yarns, the weft yarns were subjected to local bending, causing transverse cracks through the weft yarn. When the specimen was fatigue cycled to 5×10^3 cycles, debonding cracks were found to grow along the interface between adjacent binder yarns, along with transverse cracks giving rise to debonding at the cross-over area. At this stage, mutual friction took place between binder yarn and its surrounding materials, causing the interfacial damage. By 10^4 cycles, transverse cracks had become increasingly common within the weft yarns. After 5×10^4 cycles, the debonding cracks were widely spread along the path of the binder yarn, as the binder yarn became straightened under remote tensile loading. By 6×10^4 fatigue cycles, damage had continued to grow in the form of interfacial debonding, rather than by generating new transverse cracks within the weft yarns, where the strain energy stored was not sufficient for further creation of new cracks.

It is interesting to observe that in this material the fatigue damage, including matrix cracking and interfacial debonding, kept developing essentially homogeneously over the entire scanned volume until 6×10^4 cycles, rather than become localized to any particular area, which could potentially trigger the ultimate failure. This may be because the repeating structure creates a distributed network of stress concentrations with load being constantly redistributed, as cracks appear giving rise to a network of evenly spaced cracks determined by the stress redistribution lengths. As a result, fatigue damage distributes evenly with the repetitive structure, a process that the strain energy preferentially releases at each stress concentration point via the formation of new crack.

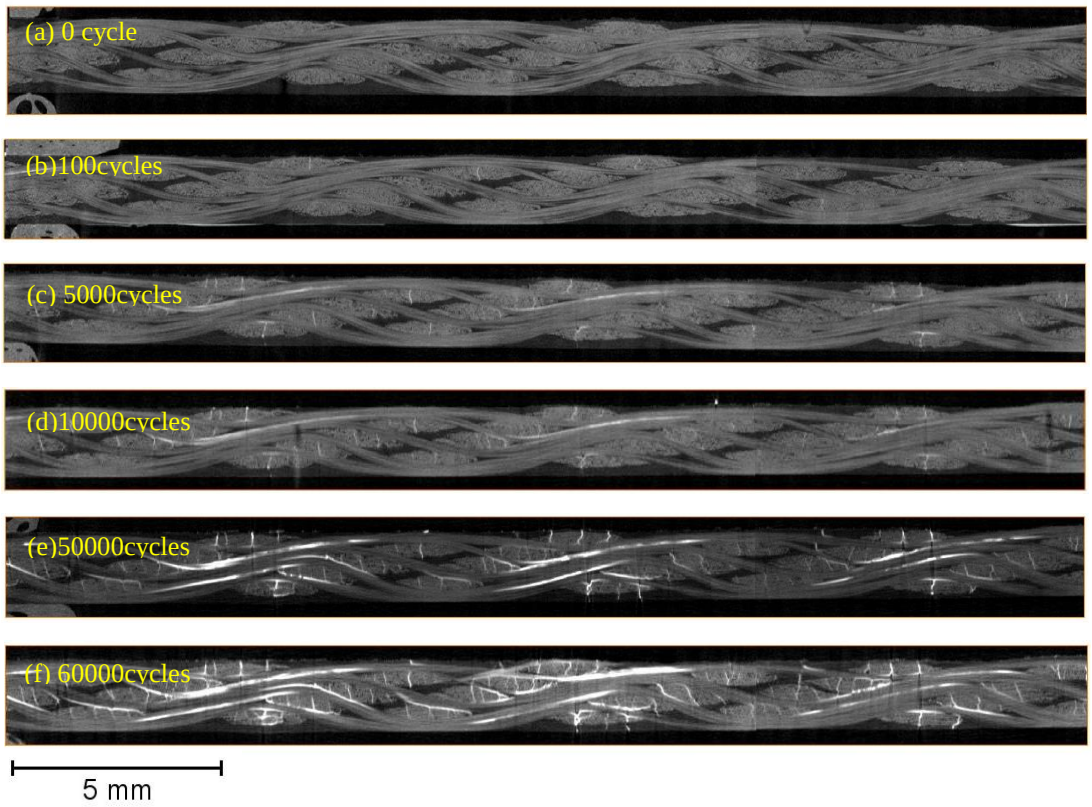

Figure 3. Images parallel to the warp direction are approximately taken from the middle orthoslices of gauge volume, showing the damage state at different number of cycles. The load is applied in the warp direction (from left to right).

As is illustrated in Fig. 4 (a) and (b), at the beginning of the fatigue life, there is no evident damage observed in cross-section normal to warp direction. As the specimen experiences more fatigue cycles, debonding cracks start to develop along the boundary of the binder yarns, which facilitates the stretching of the binder yarns with less constraint from the surrounding materials. When the specimen was cyclic loaded to 6×10^4 cycles, cracks had grown extensively between the binder yarns, suggesting that they may have experienced relative movement between each other, causing further detachment of the binder yarns.

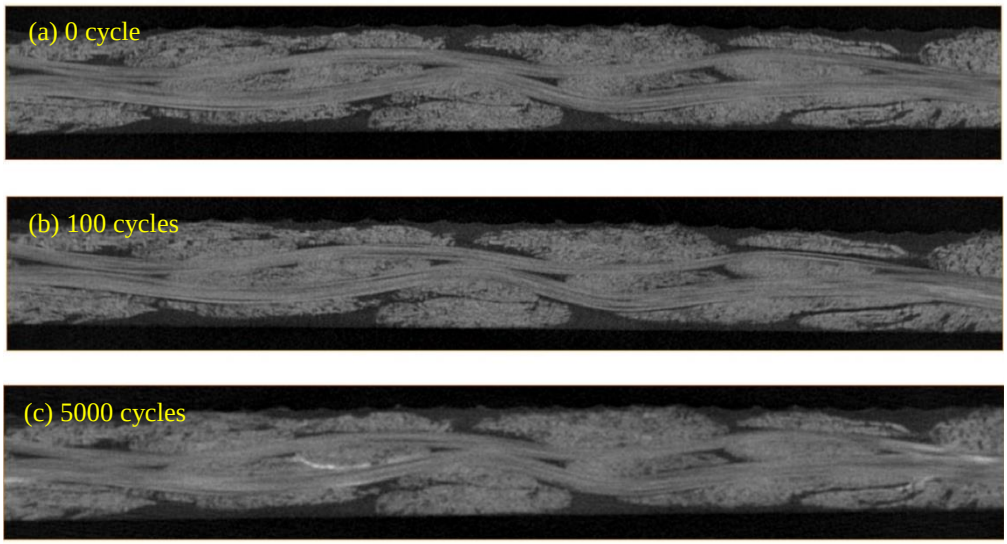

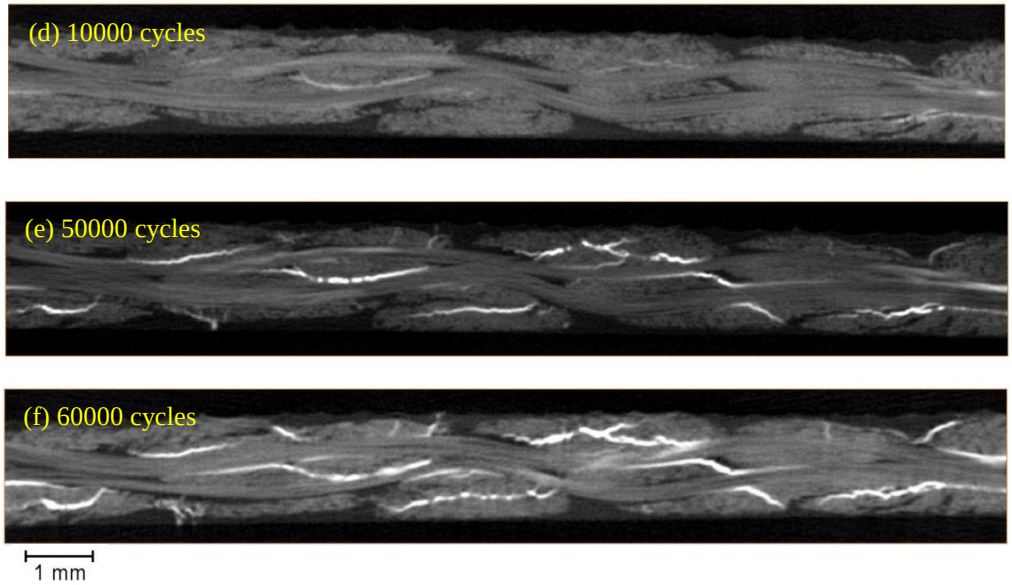

Figure 4. Images parallel to the weft direction are approximately taken from the middle orthoslices of gauge volume, showing the damage state at different number of cycles. (loading direction out of the page)

At the point of writing, the specimen has experienced 6.5×10^4 cycles but has not failed. A CT scan was performed at 6×10^4 cycles, which is in the range of typical failure life of such specimens. Therefore, the damage state at this point therefore can be considered to be close to the final stage of fatigue life. At any rate, it can be seen that the material has been severely damaged at this stage. It is worth noting that the residual stiffness has been measured to be 17.39 MPa, representing a 14% loss compared to the original sample stiffness. This indicates that while fibre breakage has not been observed in the specimen, the axial stiffness has been degraded by the existence of matrix cracking and binder debonding. This suggests that extensive debonding between binder yarns can be regarded as a precursor to specimen failure. As the binder yarns gradually lose their constraining capability, one might expect the composite to strain increasingly heterogeneously, shortly giving rise to final fracture.

Conclusions

X-ray CT has been used to monitor a 3D woven modified layer-to-layer composite specimen at different fatigue intervals to follow the accumulation of damage. It was found that fatigue damage originated from matrix cracking within weft yarns, before extending along the interface between binder and weft yarns. Debonding cracks between binder yarn and its surrounding occurred, when the inelastic straightening of binder yarns formed under cycling. It is of interest to note that the fatigue damage formed a regular pattern, until the material was extensively damaged. It is reasonable to believe that the regular tow waviness of this 3D woven structure played a key role in preventing damage localization. The quantitative assessment of the damage evolution is on-going and will be published at a later stage.

Acknowledgement

The authors wish to thankfully acknowledge all the staff in the North West Composite Centre for helpful guidance during experimental work, as well as the staff in Henry Moseley X-ray Imaging Lab, where the X-ray CT work was carried out. We are grateful to the Engineering and Physical Science Research Council (EPSRC) [grants EP/F007906/1 and EP/F028431/1]

for funding the Henry Moseley X-ray imaging facility. This work was supported by the Engineering and Physical Sciences Research Council [grant number: EP/IO33513/1], through the EPSRC Centre for Innovative Manufacturing in Composites (CIMComp). The authors gratefully appreciate the Aerospace Research Institute for assisting with the conference registration fee.

Reference

[1] A. P. Mouritz and B. N. Cox. A mechanistic interpretation of the comparative in-plane mechanical properties of 3D woven, stitched and pinned composites. *Composites Part A: Applied Science and Manufacturing,* 41(6):709-728, 2010.

[2] S. Rudov-Clark and A. P. Mouritz. Tensile fatigue properties of a 3D orthogonal woven composite. *Composites Part A: Applied Science and Manufacturing,* 39(6):1018-1024, 2008.

[3] A. P. Mouritz. Tensile fatigue properties of 3D composites with through-thickness reinforcement. *Composites Science and Technology,* 68(12):2503-2510, 2008.

[4] P. J. Callus, A. P. Mouritz, M. K. Bannister and K. H. Leong. Tensile properties and failure mechanisms of 3D woven GRP composites. *Composites Part A: Applied Science and Manufacturing,* 30(11):1277-1287, 1999.

[5] K. H. Tsai, C. H. Chiu and T. H. Wu. Fatigue behavior of 3D multi-layer angle interlock woven composite plates. *Composites Science and Technology,* 60(2):241-248, 2000.

[6] R. K. Fruehmann, J. M. Dulieu-Barton and S. Quinn. Assessment of fatigue damage evolution in woven composite materials using infra-red techniques. *Composites Science and Technology,* 70(6):937-946, 2010.

[7] D. S. Ivanov, S. V. Lomov, A. E. Bogdanovich, M. Karahan and I. Verpoest. A comparative study of tensile properties of non-crimp 3D orthogonal weave and multi-layer plain weave E-glass composites. Part 2: Comprehensive experimental results. *Composites Part A: Applied Science and Manufacturing,* 40(8):1144-1157, 2009.

[8] P. J. Withers and M. Preuss. Fatigue and Damage in Structural Materials Studied by X-Ray Tomography. *Annual Review of Materials Research, Vol 42,* 42(81-103, 2012.

[9] J. Lambert, A. R. Chambers, I. Sinclair and S. M. Spearing. 3D damage characterisation and the role of voids in the fatigue of wind turbine blade materials. *Composites Science and Technology,* 72(2):337-343, 2012.

[10] J. Stein, R.S. Bradley, B. Yu, C. Soutis, P.J. Withers. A Three Dimensional Damage Characterisation of Composites Loaded in Tension-Tension Fatigue: A Laboratory X-ray Computed Tomography Investigation In*5th conference on industrial computed tomography,* 2014.

[11] K. Vallons, M. Zong, S. V. Lomov and I. Verpoest. Carbon composites based on multi-axial multi-ply stitched preforms – Part 6. Fatigue behaviour at low loads: Stiffness degradation and damage development. *Composites Part A: Applied Science and Manufacturing,* 38(7):1633-1645, 2007.